Journal for ImmunoTherapy of Cancer

BHLHE22 drives the immunosuppressive bone tumor microenvironment and associated bone metastasis in prostate cancer

Chi Yin,[1,2] Min Wang,[1,2] Yingzhao Wang,[3] Qijun Lin,[1,2] Kaiyuan Lin,[1,2] Hong Du,[4] Chuandong Lang,[1,2] Yuhu Dai,[1,2] Xinsheng Peng [1,2]

To cite: Yin C, Wang M, Wang Y, *et al*. BHLHE22 drives the immunosuppressive bone tumor microenvironment and associated bone metastasis in prostate cancer. *Journal for ImmunoTherapy of Cancer* 2023;**11**:e005532. doi:10.1136/jitc-2022-005532

► Additional supplemental material is published online only. To view, please visit the journal online (http://dx.doi.org/10.1136/jitc-2022-005532).

CY and MW contributed equally.

Accepted 07 March 2023

For numbered affiliations see end of article.

Correspondence to
Dr Xinsheng Peng;
pengxsh@mail.sysu.edu.cn

Dr Yuhu Dai;
daiyh5@mail.sysu.edu.cn

Dr Chuandong Lang;
langchd@ustc.edu.cn

ABSTRACT

Background The molecular characteristics of prostate cancer (PCa) cells and the immunosuppressive bone tumor microenvironment (TME) contribute to the limitations of immune checkpoint therapy (ICT). Identifying subgroups of patients with PCa for ICT remains a challenge. Herein, we report that basic helix-loop-helix family member e22 (BHLHE22) is upregulated in bone metastatic PCa and drives an immunosuppressive bone TME.

Methods In this study, the function of BHLHE22 in PCa bone metastases was clarified. We performed immunohistochemical (IHC) staining of primary and bone metastatic PCa samples, and assessed the ability to promote bone metastasis in vivo and in vitro. Then, the role of BHLHE22 in bone TME was determined by immunofluorescence (IF), flow cytometry, and bioinformatic analyses. RNA sequencing, cytokine array, western blotting, IF, IHC, and flow cytometry were used to identify the key mediators. Subsequently, the role of BHLHE22 in gene regulation was confirmed using luciferase reporter, chromatin immunoprecipitation assay, DNA pulldown, co-immunoprecipitation, and animal experiments. Xenograft bone metastasis mouse models were used to assess whether the strategy of immunosuppressive neutrophils and monocytes neutralization by targeting protein arginine methyltransferase 5 (PRMT5)/colony stimulating factor 2 (CSF2) could improve the efficacy of ICT. Animals were randomly assigned to treatment or control groups. Moreover, we performed IHC and correlation analyses to identify whether BHLHE22 could act as a potential biomarker for ICT combination therapies in bone metastatic PCa.

Results Tumorous BHLHE22 mediates the high expression of CSF2, resulting in the infiltration of immunosuppressive neutrophils and monocytes and a prolonged immunocompromised T-cell status. Mechanistically, BHLHE22 binds to the *CSF2* promoter and recruits PRMT5, forming a transcriptional complex. PRMT5 epigenetically activates *CSF2* expression. In a tumor-bearing mouse model, ICT resistance of Bhlhe22$^+$ tumors could be overcome by inhibition of Csf2 and Prmt5.

Conclusions These results reveal the immunosuppressive mechanism of tumorous BHLHE22 and provide a potential ICT combination therapy for patients with BHLHE22$^+$ PCa.

WHAT IS ALREADY KNOWN ON THIS TOPIC

⇒ Bone metastatic prostate cancer (PCa) has traditionally been considered an 'immune desert', resulting in poor immune checkpoint therapy (ICT) responses.

⇒ Immunosuppressive myeloid cells are recognized to play an important role in immune evasion of PCa cells.

WHAT THIS STUDY ADDS

⇒ Targeting basic helix-loop-helix family member e22 (BHLHE22)-dependent immunosuppressive neutrophils and monocytes infiltration reduces immune checkpoint therapy (ICT) resistance and provides a potential combination therapy for patients with bone metastatic PCa.

⇒ BHLHE22 serve as a novel biomarker to select the appropriate patients with bone metastatic PCa for ICT.

HOW THIS STUDY MIGHT AFFECT RESEARCH, PRACTICE OR POLICY

⇒ Therapeutic inhibition of colony stimulating factor 2 or protein arginine methyltransferase 5, combined with anti-programmed cell death 1 therapy, could be explored as effective treatment regimens for patients with BHLHE22$^+$ PCa.

INTRODUCTION

Bone is the most common site of distant metastasis in advanced prostate cancer (PCa).[1] Within the bone tumor microenvironment (TME), unique bone marrow niches and myeloid cells contribute to metastasis, colonization, dormancy, activation, and immune escape.[2–4] Over past decades, the diagnosis rate for advanced PCa has increased from 3.9% to 8.2%.[5] Up to 90% of patients with advanced PCa have bone metastases.[6 7] There are limited therapeutic interventions for advanced PCa, including androgen deprivation therapy (ADT), biological targeted therapy, and bone targeted drug therapy, and

ultimately, PCa undergoes bone metastatic progression to become a lethal disease.[8–11]

Immune checkpoint therapy (ICT) has been proven to be effective against multiple solid tumors.[12 13] However, bone metastatic PCa has traditionally been considered an 'immune desert', resulting in poor ICT responses.[14 15] In a phase III trial of ipilimumab (NCT01057810), patients with bone metastasis responded poorly compared with those without bone metastasis.[16] Recently, a phase III clinical trial of atezolizumab (NCT03016312) demonstrated that the primary endpoint of improved overall survival was not met in unselected patients with metastatic PCa.[17] To further analyze potential biomarkers, CXCL9, TAP1, PTEN status, PD-L1, and CD8 expression levels predicted longer progression-free survival.[17] There is an urgent need to accelerate precision medicine for patients with bone metastatic PCa, including a validated selection procedure to identify subgroups of patients who might benefit from ICT.

BHLHE22 is a member of the basic helix-loop-helix (bHLH) transcription factor superfamily.[18] Peak expression of bHLH family member e22 (BHLHE22) was associated with the transformational progression of advanced PCa cells.[19] However, the function of tumorous BHLHE22 in bone metastatic PCa is unknown. In this study, we found that BHLHE22 was highly expressed in the bone metastases of patients with PCa. The tumorous BHLHE22-protein arginine methyltransferase 5 (PRMT5) transcriptional complex induces the expression and secretion of colony stimulating factor 2 (CSF2), resulting in the increase of tumor-infiltrating immunosuppressive neutrophils and monocytes. The exhaustion of $CD4^+$ T and $CD8^+$ T cells triggered by immature neutrophils and monocytes created an immunosuppressive bone TME. Treatment of tumorous Bhlhe22-expressing mice with the Csf2 or Prmt5 antagonists decreased tumor-infiltrating immunosuppressive neutrophils and monocytes, relieved the associated immunosuppressive phenotype, and enhanced the ICT response rate. Thus, our study revealed that the BHLHE22 expression level is a predictor for ICT efficacy, and revealed a prospective therapy for bone metastatic PCa.

MATERIALS AND METHODS

The complete experimental protocols are described in the online supplemental material.

RESULTS

BHLHE22 is upregulated in PCa tissues with bone metastasis and is further increased in metastatic bone tissues

To investigate the potential role of BHLHE22 in PCa metastasis, we examined the clinical significance of BHLHE22 expression in 222 PCa specimens using immunohistochemical (IHC) staining. We found a significant increase of BHLHE22 expression in primary PCa with bone metastasis (PCa/BM) compared with primary PCa without bone metastasis (PCa/nBM), and it was further upregulated in BM tissues (figure 1A). Then, we analyzed the human PCa expression profile GSE77930 and found that *BHLHE22* expression was significantly upregulated in metastatic bone tissues in contrast to that in primary PCa and other viscera metastatic sites (figure 1B). Further analysis based on The Cancer Genome Atlas (TCGA-PRAD) data set revealed that *BHLHE22* expression was markedly increased in PCa/BM compared with that in PCa/nBM (figure 1C). Moreover, Kaplan-Meier analyses based on TCGA-PRAD demonstrated that high *BHLHE22* expression predicted shorter disease-free survival (figure 1D). Consistently, upregulated *BHLHE22* expression predicted poor clinicopathological features (online supplemental table S1) and shorter overall and BM-free survival (figure 1E,F). Collectively, these results suggested that the high expression of BHLHE22 correlates to BM and poor prognosis in patients with PCa.

BHLHE22 promotes BM in an immune-associated manner

To explore the biological function of BHLHE22 in PCa, we constructed a BM mouse model by left cardiac ventricle (LCV) injection of luciferase-labeled PCa cells. Bone metastases were monitored using bioluminescent imaging (BLI) in vivo. *Bhlhe22* overexpression in RM-1 cells significantly promoted tumor BM in syngeneic C57BL/6J mice (figure 1G), but not in immunodeficient BALB/c nude mice (online supplemental figure 1A,B). Simultaneously, in immunodeficient BALB/c nude mice, there was no significant difference in BM after *BHLHE22* overexpression in PC-3 cells (online supplemental figure 1C,D). Then, the BM was confirmed by H&E and the osteolytic lesions were quantified using micro-CT scan (figure 1H,I). Micro-CT analysis showed that BHLHE22 contributed to a larger osteolytic bone lesion area (figure 1J,K). Survival analysis demonstrated that overexpression of *BHLHE22* predicted shorter overall and BM-free survival (figure 1L,M). Additionally, we evaluated the role of BHLHE22 in vitro. Transwell migration/invasion assays indicated no significant difference between *BHLHE22* overexpression and vector cells (online supplemental figure 1E,F). Taken together, BHLHE22 drives a disparate BM phenotype between immunocompetent and immunodeficient mice. Consistently, BHLHE22 caused phenotypic differences between in vivo and in vitro assays. Hence, we hypothesized that the differential effects on BM status by BHLHE22 might be caused by its effects on the tumorous bone immune microenvironment.

To assess these effects, we performed a gene set enrichment analysis (GSEA) of the TCGA-PRAD data sets according to *BHLHE22* expression to identify its regulated signaling pathways. Patients were stratified by low (bottom 50% quantile) and high (top 50% quantile) *BHLHE22* expression. Interestingly, the GSEA analysis showed that negative regulation of immune response and negative regulation of interferon (IFN)-γ production pathways were activated in *BHLHE22*-high patients (online supplemental figure 1G). In addition,

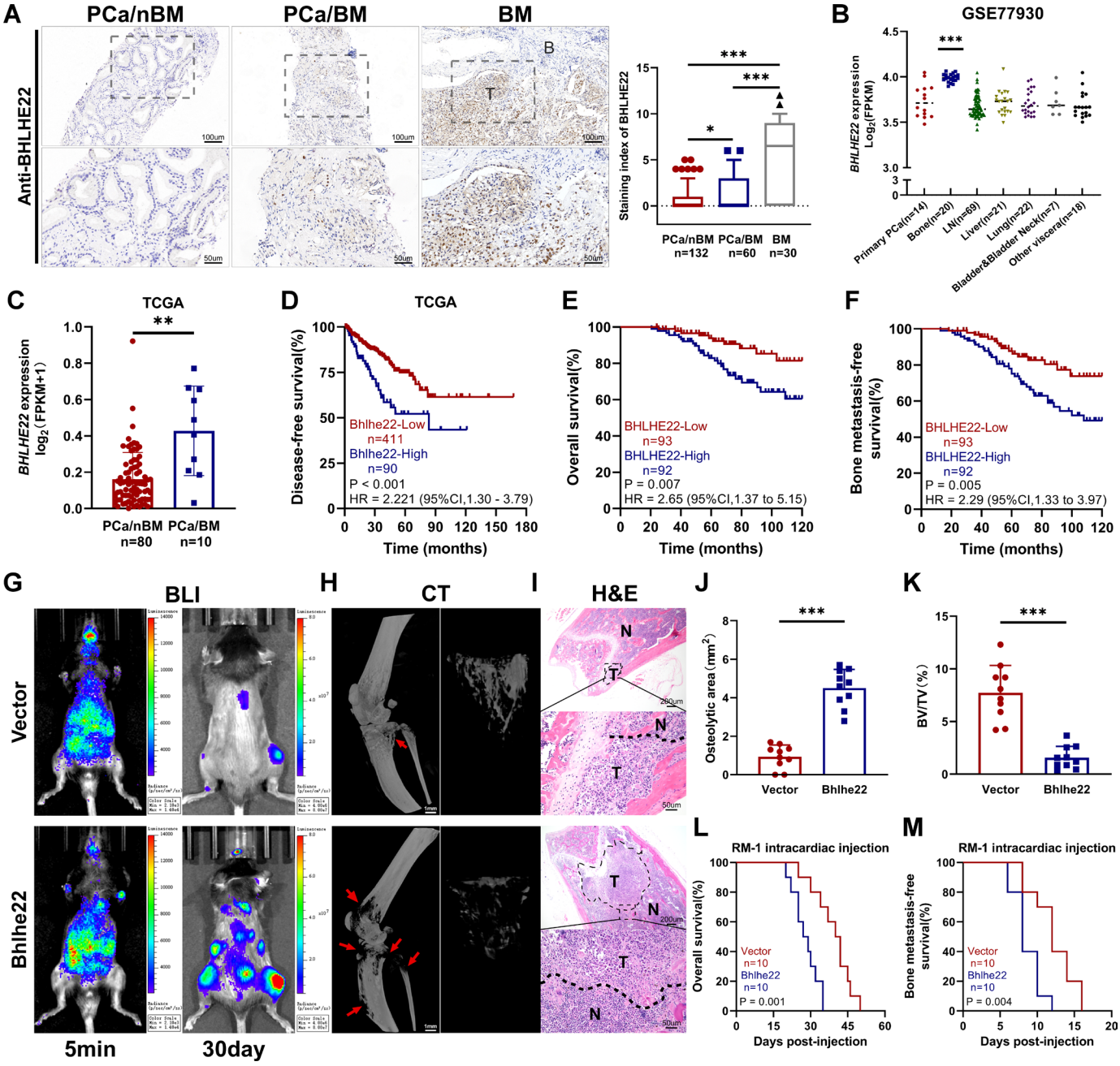

Figure 1 BHLHE22 is upregulated in PCa with bone metastasis and promotes bone metastasis. (A) Representative images and quantification of immunohistochemical staining of BHLHE22 expression in human PCa/nBM (n=132), PCa/BM (n=60) and BM (n=30). T, tumor; B, bone tissue. Bars, 100 µm and 50 µm. *p<0.05, ***p<0.001; one-way analysis of variance (ANOVA). (B) *BHLHE22* expression in metastatic bone tissues, primary prostate, and other viscera metastatic sites from GSE77930. ***p<0.001; one-way ANOVA. (C) *BHLHE22* expression in PCa/nBM and PCa/BM from the TCGA-PRAD data set. **p<0.01; Mann-Whitney test. (D) Kaplan-Meier analysis of disease-free survival curves in the TCGA-PRAD data set stratified by low and high *BHLHE22* expression. The cut-off value was selected based on ROC curve. p<0.001; log-rank test. (E) Kaplan-Meier analysis of overall survival curves of patients with PCa stratified by low (bottom 50% quantile) and high (top 50% quantile) BHLHE22 expression. p=0.007; log-rank test. (F) Kaplan-Meier analysis of bone metastasis-free survival curves of patients with PCa stratified by low (bottom 50% quantile) and high (top 50% quantile) BHLHE22 expression. p=0.005; log-rank test. (G) Representative BLI signal of bone metastasis of left cardiac ventricle-injected C57BL/6J mice. (H) Representative micro-CT images of bone lesions (arrows indicate osteolytic lesions) and trabecular sections. Bars, 1 mm. (I) H&E-stained sections of the posterior limbs (T, tumor; N, the adjacent non-tumor tissues). Bars, 200 µm and 50 µm. (J) Quantification of osteolytic areas. ***p<0.001; t-test. (K) Quantification of bone parameters. BV/TV, bone/tissue volume ratio. ***p<0.001; t-test. (L and M) Kaplan-Meier analysis of overall (L) and bone metastasis-free (M) survivals. p=0.001 (L) and p=0.004 (M); log-rank test. BHLHE22, basic helix-loop-helix family member e22; ROC, Receiver operating characteristic; BLI, bioluminescent imaging; PCa/BM, PCa with bone metastasis; PCa/nBM, PCa without bone metastasis; PCa, prostate cancer; TCGA, The Cancer Genome Atlas.

RNA transcriptome sequencing (RNA-seq) analysis was performed on three paired PC-3-BHLHE22 and PC-3-Vector cells. GSEA analysis of the RNA-seq data showed that negative regulation of immune response and negative regulation of T cell-mediated immunity pathways were activated in PC-3-BHLHE22 cells (online supplemental figure 1G). Gene Ontology analysis revealed that an immune response gene signature was the top enrichment term (online supplemental figure 1H). Moreover, the cell cycle and DNA replication gene signatures were also enriched. Therefore, we examined whether *BHLHE22* overexpression affected cell proliferation. Interestingly, our results showed that cell viability increased after *BHLHE22* overexpression in PC-3 cells, whereas RM-1 cells were not affected (online supplemental figure 1I-K). The above results suggested that BHLHE22 functions in an immunity-associated manner to promote BM.

BHLHE22 drives an immunosuppressive TME in BM

To determine whether and how BHLHE22 affects the PCa bone immune microenvironment, we investigated the infiltration of immunosuppressive myeloid cells, including immature neutrophils and monocytes, and $CD8^+$ T cells in our PCa specimens. Immunosuppressive myeloid cells were defined as the $CD33^+$ cells in human tissue samples.[20] Immunosuppressive neutrophils and monocytes were defined as the $CD11b^+Gr1^+$ cells, which can be further classified into $CD11b^+Ly6C^{lo}Ly6G^+$ (neutrophils) and $CD11b^+Ly6C^{hi}Ly6G^-$ (monocytes).[21] Tissue immunofluorescence (IF) of CD33, CD8, BHLHE22, and 4′,6-diamidino-2-phenylindole staining were performed in PCa/BM and BM tissues (figure 2A,B). The results suggested that the BHLHE22-high group had more $CD33^+$ cells infiltration than the BHLHE22-low group in PCa/BM and BM tissues. The BHLHE22-low group had higher $CD8^+$ T-cell infiltration than the BHLHE22-high group (figure 2D,E). Then, we examined tumor-infiltrating $CD11b^+Gr\text{-}1^+$ cells, and $CD4^+$ T and $CD8^+$ T cells in C57BL/6J mice bone marrow samples that were LCV-injected with RM-1-Bhlhe22 and RM-1-Vector cells. The RM-1-Bhlhe22 group had markedly increased $CD11b^+Gr\text{-}1^+$ cells infiltration and decreased $CD4^+$ T and $CD8^+$ T-cell infiltration in bone marrow compared with that in the RM-1-Vector group (figure 2C,F).

To further confirm the effects of BHLHE22 in the bone TME, the BM bone marrow samples of C57BL/6J mice LCV-injected with RM-1-Vector or RM-1-Bhlhe22 cells were collected simultaneously and subjected to immune profiling using flow cytometry. The proportions of $CD45^+$ $7AAD^-$ cells and $CD3^+CD11b^-$ cells in the RM-1-Bhlhe22 and the RM-1-Vector groups were comparable (p=0.803 and p=0.835; online supplemental figure 2A,B). The relative proportions of $CD11b^+Gr\text{-}1^+$ cells, including monocytes and neutrophils, $CD4^+$ T, $CD8^+$ T, γ/δ T cells, regulatory T (Tregs), M1 and M2 macrophages, and natural killer (NK) cells in $CD45^+7AAD^-$ cells were evaluated. Consistently, the RM-1-Bhlhe22 group showed notably increased $CD11b^+Gr\text{-}1^+$ cells infiltration, specifically monocytes, and decreased $CD4^+$ T and $CD8^+$ T cells infiltration compared with those in the RM-1-Vector group (figure 2G–J). However, no significant difference was observed in the percentage of γ/δ T cells, Tregs, M1 and M2 macrophages, and NK cells (online supplemental figure 2C–F). Furthermore, key immune function-related factors were investigated, including arginase-1 (Arg-1), IFN-γ, and programmed cell death 1 (PD-1). The RM-1-Bhlhe22 group exhibited a higher proportion of $Arg\text{-}1^+Gr\text{-}1^+$ cells (figure 2G,H) and $PD\text{-}1^+CD8^+$ T cells, and lower percentages of $IFN\text{-}\gamma^+CD8^+$ T cells (figure 2I,K). In addition, to examine whether these $CD11b^+Gr\text{-}1^+$ cells are indeed functional immunosuppressive myeloid cells, we performed a standard T-cell co-culture proliferation-suppression assay. Isolated $CD11b^+Gr\text{-}1^+$ cells were co-cultured with $CD8^+$ T cells in varying proportions: $CD11b^+Gr\text{-}1^+$ cells strongly suppressed CD3 and CD28 antibody-induced T-cell proliferation and activation after 4 days of co-culture (figure 2L,M). We performed another $CD11b^+Gr\text{-}1^+$ cells depletion assay in vivo. When the RM-1-Bhlhe22 group was treated with anti-Gr-1 antibodies, the percentage of $CD11b^+Gr\text{-}1^+$ cells decreased significantly and the percentage of $CD4^+$ T and $CD8^+$ T cells increased significantly (online supplemental figure 2G). The exhaustion of $CD4^+$ T and $CD8^+$ T cells triggered by $CD11b^+Gr\text{-}1^+$ cells was reversed by the depletion. Collectively, we concluded that $CD11b^+Gr\text{-}1^+$ cells induced by BHLHE22-high PCa cells drive an immunosuppressive TME by exhausting T cells.

BHLHE22 controls immunosuppressive neutrophils and monocytes recruitment and CSF2 serves as a key mediator

Next, we determined how the differences in immune profiling occurred. The crosstalk between cancer cells and tumor-infiltrating immune cells is often mediated by direct cell–cell interaction and secretory factors, such as cytokines and chemokines.[22] Thus, we analyzed our RNA-seq data sets from RM-1-Bhlhe22 and PC-3-BHLHE22 cells compared with vector cells, respectively. We identified 103 co-upregulated genes and 37 co-downregulated genes (fold-change >1.5) (online supplemental figure 3A). Surprisingly, *CSF2* was the only secretory factor gene that was co-upregulated in RM-1-Bhlhe22 and PC-3-BHLHE22 cells (figure 3A).

The cytokine array analysis showed that RM-1-Bhlhe22 cells secreted a higher amount of Csf2 than RM-1-Vector cells (figure 3B). Western blotting demonstrated higher Csf2 levels in the RM-1-Bhlhe22 group (including cell lines and BM tissues of C57BL/6J mice) (figure 3C,D). The relationship between Csf2 expression and immune cell infiltration, including immunosuppressive myeloid cells ($Gr\text{-}1^+$, $S100A9^+$), $CD4^+$ T and $CD8^+$ T cells, was detected in LCV-injected C57BL/6J mice BM tumor samples. The *Bhlhe22* overexpression group had higher $Gr\text{-}1^+$ and $S100A9^+$ cells counts, and lower $CD4^+$ T and $CD8^+$ T cells counts per high-power field (HPF; 400×), and higher Csf2 levels compared with those in the vector group (figure 3E–H). Correlation analysis of

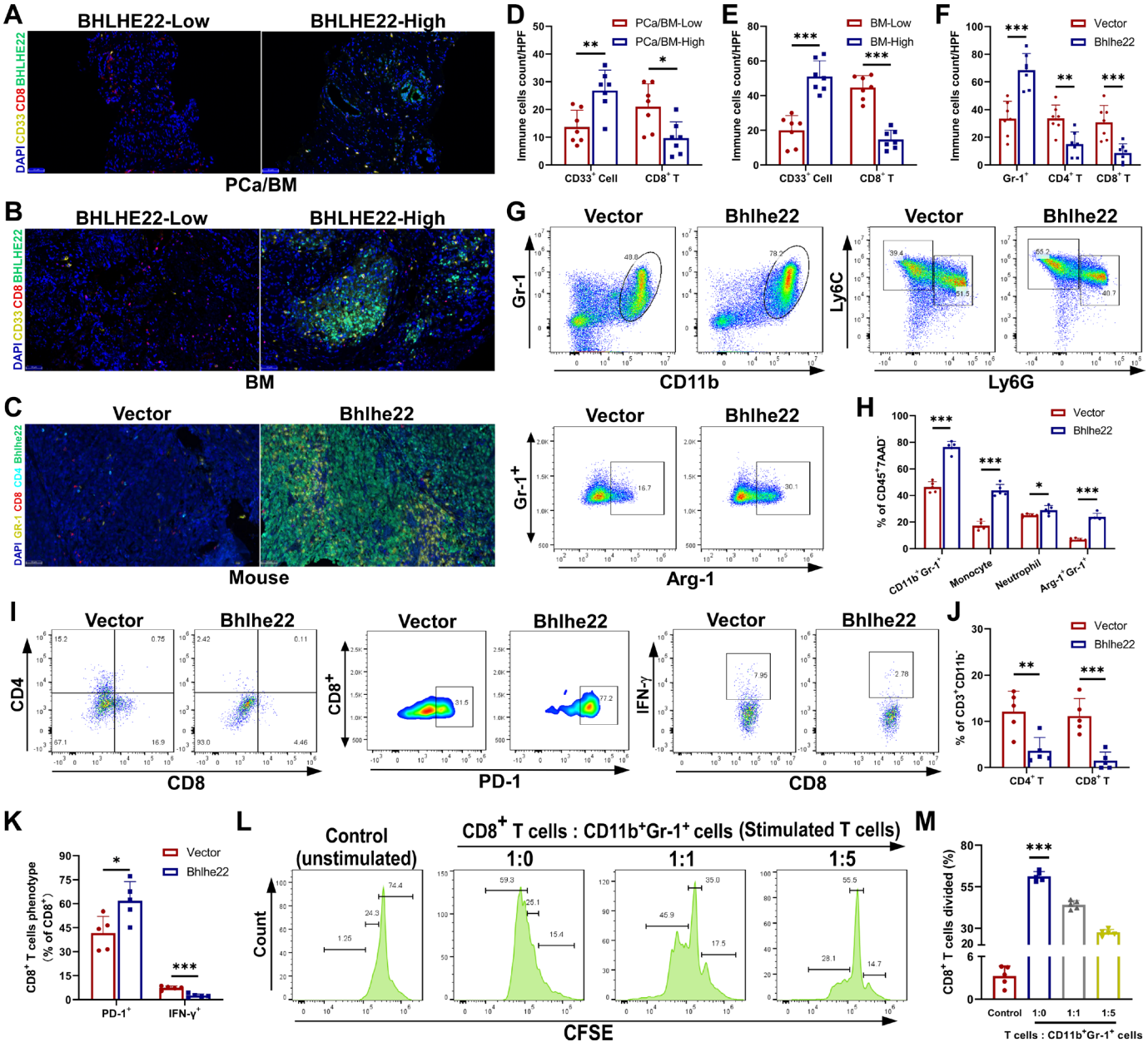

Figure 2 BHLHE22 drives an immunosuppressive tumor microenvironment in bone metastasis. (A and B) Representative IF staining images of BHLHE22 expression and the infiltration of $CD33^+$ cells and $CD8^+$ T cells in PCa/BM (A) and BM (B) tissues. Samples were stratified by low (bottom 50% quantile) and high (top 50% quantile) BHLHE22 expression. Bars, 50 µm. (C) Representative IF staining images of Bhlhe22 expression and the infiltration of $CD4^+$ T and $CD8^+$ T cells, and $Gr\text{-}1^+$ cells in LCV-injected mouse bone marrow. Bars, 50 µm. (D and E) Quantification of $CD33^+$ cells and $CD8^+$ T cells per high-power field in human PCa/BM (D) and BM (E). *p<0.05, **p<0.01, ***p<0.001; t-test. (F) Quantification of $CD4^+$ T and $CD8^+$ T cells, and $Gr\text{-}1^+$ cells per high-power field in LCV-injected mice bone marrow. **p<0.01, ***p<0.001; t-test. (G) Flow cytometry showing numbers of $CD11b^+Gr\text{-}1^+$ cells, $CD11b^+Ly6C^{hi}Ly6G^-$ (monocytes), $CD11b^+Ly6C^{lo}Ly6G^+$ (neutrophils), and $Gr\text{-}1^+Arg\text{-}1^+$ cells in LCV-mice bone marrow. (H) Quantification of tumor-infiltrating $CD11b^+Gr\text{-}1^+$ cells, monocytes, neutrophils, and $Arg\text{-}1^+Gr\text{-}1^+$ cells. *p<0.05, ***p<0.001; t-test. (I) Flow cytometry showing numbers of $CD4^+$ T, $CD8^+$ T, $PD\text{-}1^+CD8^+$ T, and $IFN\text{-}\gamma^+CD8^+$ T cells in LCV-mice bone marrow. (J and K) Quantification of tumor-infiltrating $CD4^+$ T cells, $CD8^+$ T cells (J), $PD\text{-}1^+CD8^+$ T cells, and $IFN\text{-}\gamma^+CD8^+$ T cells (K). *p<0.05, **p<0.01, ***p<0.001; t-test. (L and M) Representative CFSE flow-cytometry histograms and summarized results showing $CD8^+$ T-cell proliferation induced by isolated $CD11b^+Gr\text{-}1^+$ cells from $Bhlhe22^+$ BM mouse samples. ***p<0.001; t-test. Arg-1, arginase-1; BHLHE22, basic helix-loop-helix family member e22; BM, bone metastasis; CFSE, carboxyfluorescein succinimidyl ester; HPF, high-power field; IF, immunofluorescence; IFN, interferon; LCV, left cardiac ventricle; PCa/BM, PCa with bone metastasis; PCa, prostate cancer; PD-1, programmed cell death 1.

$Csf2^+$ and $Gr\text{-}1^+$ cells showed that Csf2 expression positively correlated with $Gr\text{-}1^+$ cells infiltration (r=0.645, p<0.001; figure 3H). Positive staining for the Ki-67 proliferation marker indicated that Bhlhe22-induced tumor-infiltrating $CD11b^+Gr\text{-}1^+$ cells facilitate BM outgrowth in mice (figure 3I and online supplemental

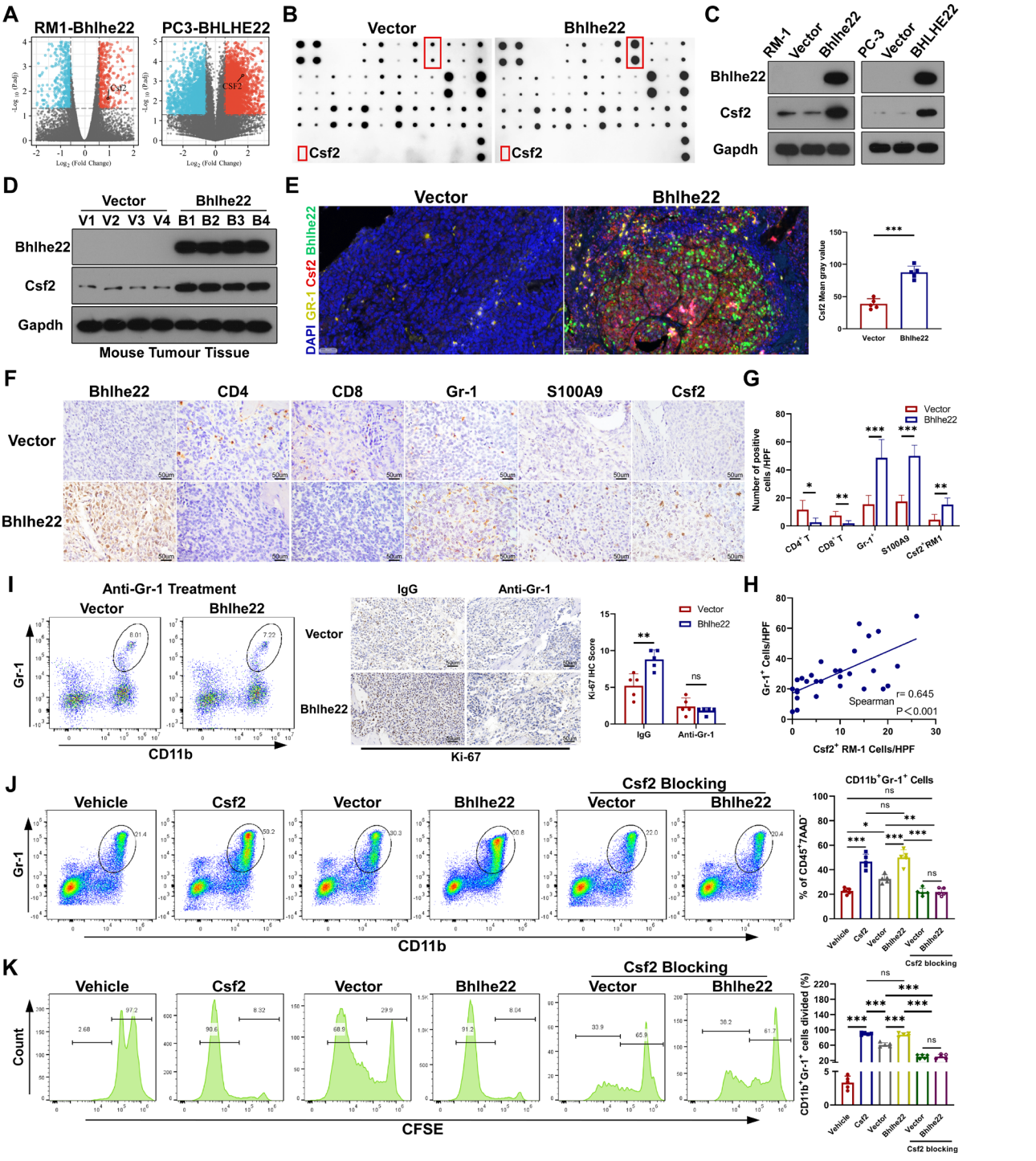

Figure 3 BHLHE22 controls immunosuppressive neutrophils and monocytes recruitment and CSF2 serves as a key mediator. (A) Volcano plot showing differentially expressed genes of *BHLHE22* overexpression versus Vector in RM-1 and PC-3 cells (fold-change >1.5). (B) Cytokine array examining the supernatants of RM-1-Vector and RM-1-Bhlhe22. (C) Western blotting analysis of Csf2 in cell lines. (D) Western blotting analysis of Csf2 in bone metastasis mouse tumor tissues. (E) Representative immunofluorescence staining images of Bhlhe22, Csf2, Gr-1, and quantification of Csf2 expression in LCV-injected mouse bone marrow. Bars, 50 µm. (F) IHC results showing Bhlhe22, Csf2, and $CD4^+$ T (CD4), $CD8^+$ T (CD8), immunosuppressive myeloid cells (Gr-1 and S100A9) infiltration in LCV-injected mouse bone marrow. Bars, 50 µm. (G) IHC results showing numbers of positive cells per high-power field. *p<0.05, **p<0.01, ***p<0.001; t-test. (H) Spearman correlation analysis between $Csf2^+$ and $Gr\text{-}1^+$ cells. (I) Representative pseudo-color plots of $CD11b^+Gr\text{-}1^+$ cells, and IHC results of Ki-67 staining in the indicated groups with or without the depletion using anti-Gr-1 antibodies. Histogram analysis of the Ki-67 staining score. ns, not significant. **p<0.01. t-test. (J) In vivo $CD11b^+Gr\text{-}1^+$ cells infiltration analysis. ns, not significant. *p<0.05, **p<0.01, ***p<0.001; one-way analysis of variance (ANOVA). (K) Co-culture assays showing in vitro $CD11b^+Gr\text{-}1^+$ cells expansion. ns, not significant. ***p<0.001; one-way ANOVA. BHLHE22, basic helix-loop-helix family member e22; CFSE, carboxyfluorescein succinimidyl ester; CSF2, colony stimulating factor 2; HPF, high-power field; IHC, immunohistochemical; LCV, left cardiac ventricle.

figure 3B). Interestingly, in the TCGA-PRAD tumor data sets, *BHLHE22* expression correlated positively with *CSF2* expression (r=0.230, p<0.001; online supplemental figure 3C). Therefore, we hypothesized that CSF2 might be a key mediator in the immunosuppressive bone TME induced by BHLHE22$^+$ PCa.

Next, in vivo and in vitro studies were conducted to evaluate the treatment efficacy of CSF2 neutralization. For the in vivo CD11b$^+$Gr-1$^+$ cells infiltration analysis, C57BL/6J mice were LCV-injected with RM-1-Vector or RM-1-Bhlhe22 cells. Then, we treated non-tumor-bearing mice with recombinant murine Csf2 (isotype IgGs as control). LCV-injected mice were treated with anti-CSF2 antibody (isotype IgGs as control). BMs were monitored using BLI and osteolytic lesions were quantified using micro-CT scan. Previous studies have shown that CSF2 promotes osteoclastogenesis.[23] Hence, osteoclasts were evaluated by tartrate-resistant acid phosphatase (TRAP) staining (online supplemental figure 3D-F). At 30 days post-injection, bone marrow was collected for flow cytometry analysis. Similar to the non-tumor-bearing group treated with Csf2, tumorous *Bhlhe22* overexpression strongly promoted CD11b$^+$Gr-1$^+$ cells infiltration. However, anti-CSF2 antibodies significantly inhibited CD11b$^+$Gr-1$^+$ cells infiltration (figure 3J). For the in vitro CD11b$^+$Gr-1$^+$ cells expansion analysis, CD11b$^+$Gr-1$^+$ cells were isolated and labeled with carboxyfluorescein succinimidyl ester (CFSE). Isolated CD11b$^+$Gr-1$^+$ cells were co-cultured with RM-1-Vector or RM-1-Bhlhe22 cells. Non-co-cultured CD11b$^+$Gr-1$^+$ cells were used as the vehicle group. Then, we treated non-co-cultured cells with recombinant murine Csf2 (isotype IgGs as control). Co-cultured cells were treated with anti-CSF2 antibody (isotype IgGs as control). After 5 days of incubation, similar to the Csf2 group, CFSE assays demonstrated that tumorous *Bhlhe22* overexpression strongly promoted CD11b$^+$Gr-1$^+$ cells expansion. Nevertheless, anti-CSF2 antibodies significantly inhibited CD11b$^+$Gr-1$^+$ cells expansion (figure 3K). Moreover, the proportions of Ki-67$^+$CD11b$^+$Gr-1$^+$ cells were analyzed. The results showed that tumorous *Bhlhe22* overexpression significantly promoted and anti-CSF2 significantly inhibited CD11b$^+$Gr-1$^+$ cells proliferation (online supplemental figure 3G). Therefore, we concluded that CSF2 is the key mediator of BHLHE22-induced immune profile changes.

BHLHE22 and PRMT5 form a transcriptional complex and transcriptionally activate *CSF2*

BHLHE22 is a transcription factor; therefore, we sought to determine whether *CSF2* is transcriptionally regulated by BHLHE22. A luciferase reporter assay revealed that BHLHE22 increased the activity of the *CSF2* promoter in RM-1-Bhlhe22 and PC-3-BHLHE22 cells (figure 4A). To determine whether BHLHE22 binds to the *CSF2* promoter, a chromatin immunoprecipitation (ChIP) assay with anti-BHLHE22 antibodies was performed, in which the *CSF2* promoter was pulled down from RM-1-Bhlhe22 and PC-3-BHLHE22 cell lysates, and verified using PCR (online supplemental figure 4A–C). In addition, based on the JASPAR[24] and CIS-BP[25] databases, we compared the human and mouse BHLHE22 binding motifs in the *CSF2* promoter, and found the same BHLHE22 binding motifs in both organisms (online supplemental figure 4D).

BHLHE22 usually forms a transcriptional complex that works together to govern cell fate decisions in a variety of tissues.[26] Hence, we wondered whether BHLHE22 transcriptionally regulated *CSF2* expression in cooperation with other proteins. To identify the potential protein–protein interactions, a co-immunoprecipitation (co-IP) assay was carried out. The eluate and the differentially abundant bands were analyzed using mass spectrometry (MS). The MS results identified enrichment of 10 potential transcriptional cofactors (figure 4B). Meanwhile, to further confirm the BHLHE22 binding sites (BBSs) and the key cofactors, we analyzed data in JASPAR and found six high-confidence BBSs corresponding to the promoter region of *Csf2* (online supplemental figure 4E). Subsequently, we designed four 50–150 bp 5′ biotin-labeled DNA probes containing the predicted BBS in the center (online supplemental table S2). We coupled the DNA probes to magnetic beads and used uncoupled beads as the negative control. DNA pulldown assays revealed that the same differentially expressed band was found in *Csf2* promoter region P1 and P1-4 between 60 and 75 kDa, but not in P2, P3, and P4 (figure 4C). Therefore, we considered that region P1 might be responsible for Bhlhe22 binding. Further analysis of the DNA probe eluates using western blotting revealed that Prmt5 was pulled down by probes P1 and P1-4 (online supplemental figure 4F). Moreover, colocalization of Bhlhe22 and Prmt5 in the nucleus was also shown using cellular IF staining (figure 4D). To further verify whether Bhlhe22 bound to the P1 region of the *Csf2* promoter to activate gene transcription, we constructed three Csf2 luciferase promoter vectors: pGL4-FL-BBS (full length BBS), pGL4-P1-BBS-Wt (wild-type P1 region), or pGL4-P1-BBS-Mut (mutated BBS) (online supplemental table S3). Then, we transfected them into RM-1-Bhlhe22 cells and HEK293T cells (HEK293T cells were additionally co-transfected with the *Bhlhe22* expression plasmid). Luciferase analysis demonstrated that mutation of the P1 region significantly decreased *Csf2* promoter activity (figure 4E). To further identify the interaction between Bhlhe22 and Prmt5, we performed endogenous and exogenous reciprocal immunoprecipitation (IP) assays. Strikingly, both IP assays revealed that Bhlhe22 interacted with Prmt5 (figure 4F,G).

Next, we addressed how the transcriptional complex binds to the target gene and the specific binding patterns of Bhlhe22 and Prmt5 in the transcriptional complex. First, we examined the *Prmt5* expression level of the vector control and the *Bhlhe22* overexpression groups in RM-1 and PC-3 cell lines; however, there was no significant difference between these two groups (online supplemental figure 4G). Therefore, we considered that Bhlhe22

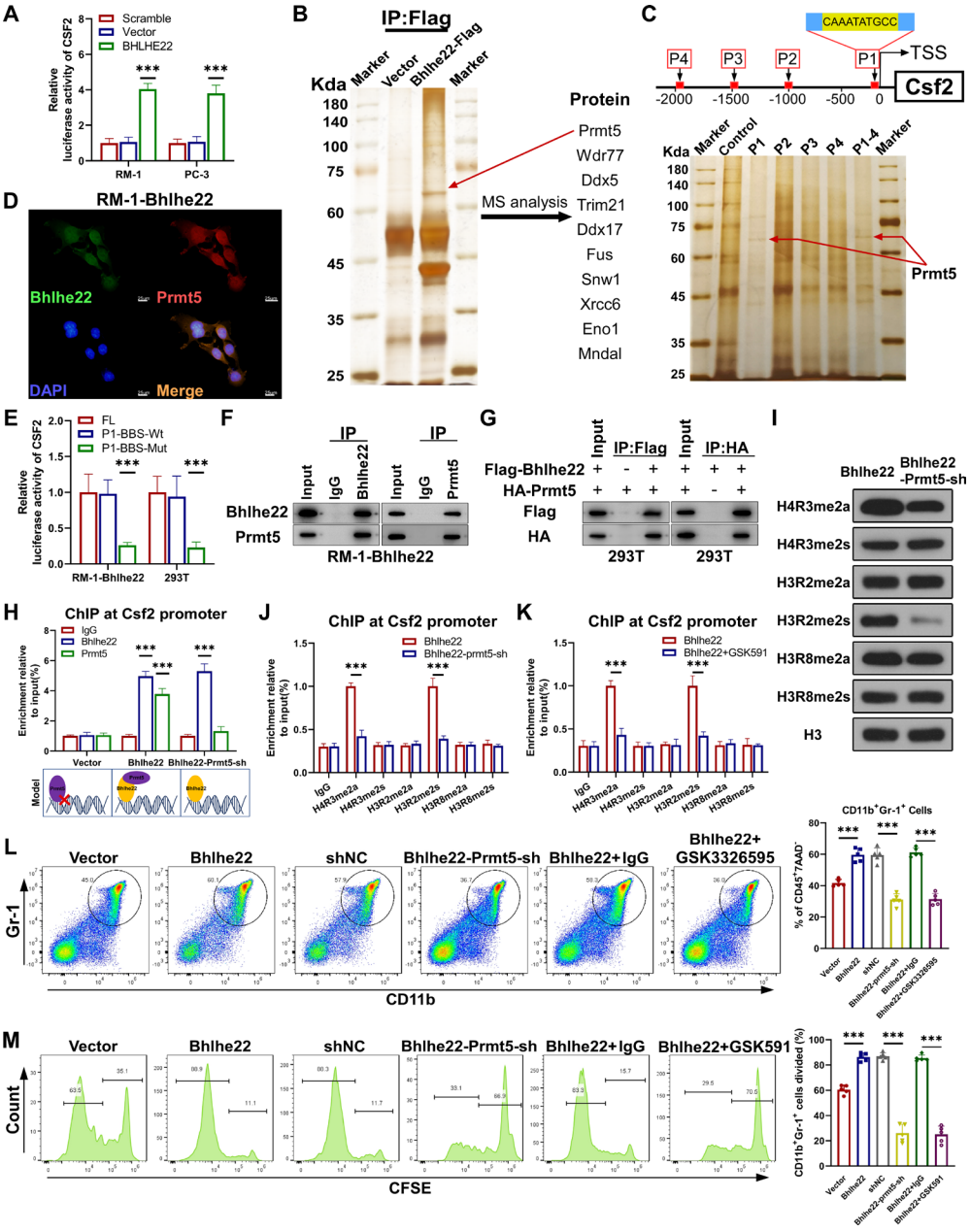

Figure 4 BHLHE22 and PRMT5 form a transcriptional complex and transcriptionally activate CSF2. (A) *CSF2* promoter activity measured by dual-luciferase reporter assay in RM-1 and PC-3 cells transduced with lentiviruses harboring control vector or *BHLHE22* overexpression. ***p<0.001; one-way analysis of variance (ANOVA). (B) Co-immunoprecipitation assay and mass spectrometry (MS) analysis were performed to detect Bhlhe22-interacting cofactors. A red arrow indicates Prmt5. (C) DNA pulldown assays to detect proteins interacting with the *Csf2* promoter. A red arrow indicates Prmt5. (D) Immunofluorescence staining of Bhlhe22 and Prmt5 to examine their colonization. Bars, 25 µm. (E) *Csf2* promoter activity measured by dual-luciferase reporter assay in HEK293T (exogenous, containing Bhlhe22 expression vector) and RM-1-Bhlhe22 (endogenous) cells transduced with pGL4-FL-BBS, pGL4-P1-BBS-WT, or pGL4-P1-BBS-mutation. ***p<0.001. one-way ANOVA. (F) IP assays determining the interaction between Bhlhe22 and Prmt5 in RM-1 cells. (G) IP assays were performed in HEK293 T cells transduced with Flag-Bhlhe22 and HA-Prmt5 constructs. (H) ChIP-qPCR analysis of Bhlhe22 and Prmt5 enrichment on the *Csf2* promoter in RM-1-Vector (*Bhlhe22*$^{-}$/*Prmt5*$^{+}$), RM-1-Bhlhe22 (*Bhlhe22*$^{+}$/*Prmt5*$^{+}$), and RM-1-Bhlhe22-Prmt5-sh (*Bhlhe22*$^{+}$/*Prmt5*$^{-}$) cells. Model diagram shown below. ***p<0.001; one-way ANOVA. (I) Western blotting analysis of symmetrically methylated H4R3, H3R2, and H3R8 in the indicated cells. (J) ChIP-qPCR analysis of symmetrically methylated H4R3, H3R2, and H3R8 enrichment on the *Csf2* promoter in RM-1-Bhlhe22 and RM-1-Bhlhe22-Prmt5-sh cells. ***p<0.001; t-test. (K) ChIP-qPCR analysis of symmetrically methylated H4R3, H3R2, and H3R8 enrichment on the *Csf2* promoter in RM-1-Bhlhe22 and RM-1-Bhlhe22 plus GSK591 cells. ***p<0.001; t-test. (L) In vivo CD11b^{+}Gr-1^{+} cells infiltration analysis. ***p<0.001; one-way ANOVA. (M) Co-culture assays showing in vitro CD11b^{+}Gr-1^{+} cells expansion. ***p<0.001. one-way ANOVA. BHLHE22, basic helix-loop-helix family member e22; CFSE, carboxyfluorescein succinimidyl ester; ChIP, chromatin immunoprecipitation; CSF2, colony stimulating factor 2; DAPI, 4′,6-diamidino-2-phenylindole; IP, immunoprecipitation; PRMT5, protein arginine methyltransferase 5; qPCR, quantitative PCR.

might not regulate *Prmt5* expression. ChIP-quantitative PCR (qPCR) was performed using three kinds of RM-1 cell lines, including RM-1-Vector (*Bhlhe22*$^{-}$/*Prmt5*$^{+}$), RM-1-Bhlhe22 (*Bhlhe22*$^{+}$/*Prmt5*$^{+}$) and RM-1-Bhlhe22-Prmt5-sh (*Bhlhe22*$^{+}$/*Prmt5*$^{-}$). We found that Prmt5 could not bind to the *Csf2* promoter in RM-1-Vector cells. In contrast, Bhlhe22 showed similar binding ability to the *Csf2* promoter when ChIP-qPCR was performed using RM-1-Bhlhe22 and RM-1-Bhlhe22-Prmt5-sh cells. However, Prmt5 displayed a strong binding ability to the *Csf2* promoter in RM-1-Bhlhe22 cells (figure 4H). In the absence of Bhlhe22, Prmt5 could not bind to the *Csf2* promoter (figure 4H, as the model diagram presented below). Thus, Prmt5's ability to bind the *Csf2* promoter depends on Bhlhe22. These results revealed that BHLHE22 binds to the *CSF2* promoter and recruits PRMT5 to form a transcriptional complex that activates *CSF2* transcription.

PRMT5 epigenetically activates *CSF2* expression

PRMT5 has been reported to act as an epigenetic modifier that regulates gene expression by methylating histones. Moreover, PRMT5 functions in transcriptional activation or repression via symmetric dimethylation of diverse histones.[27 28] We examined the Csf2 expression level by western blotting and quantitative real-time reverse transcription PCR (qRT-PCR) after knockdown of *Prmt5* in RM-1-Bhlhe22 cells. *Prmt5* knockdown induced a significant decrease in Csf2 expression (online supplemental figure 4H). We also examined the level of various symmetrically methylated histones, such as H4R3, H3R2, and H3R8. Remarkably, *Prmt5* knockdown induced a reduction of H4R3me2a and H3R2me2s levels (figure 4I). Previous studies suggested that dimethylation of H4R3 (H4R3me2a) and H3R2 (H3R2me2s) could activate gene transcription in cancer.[27 28] Subsequently, to determine whether Prmt5 could directly methylate the H4R3 and H3R2 around the *Csf2* promoter region, several ChIP assays were performed in RM-1-Bhlhe22 cells. *Prmt5* knockdown decreased the enrichment of both H4R3me2a and H3R2me2s on the *Csf2* promoter, supporting the view that the *Csf2* promoter is a dimethylation target of Prmt5 (figure 4J). Furthermore, treatment with the Prmt5 inhibitor, GSK591, significantly reduced Csf2 expression in RM-1-Bhlhe22 cells (online supplemental figure 4I). Consistently, GSK591 significantly decreased the enrichment of H4R3me2a and H3R2me2s on the *Csf2* promoter in RM-1-Bhlhe22 cells (figure 4K).

To assess the effects of Prmt5 on immunosuppressive neutrophils and monocytes infiltration, in vivo and in vitro studies were conducted to estimate the treatment efficacy of the Prmt5 inhibitor. The Prmt5 inhibitor GSK3326595 was used in vivo and GSK591 was used in vitro. For the in vivo CD11b^{+}Gr-1^{+} cells infiltration analysis, C57BL/6J mice were LCV-injected with RM-1-Vector or RM-1-Bhlhe22 or RM-1-Bhlhe22-Prmt5-sh cells (plus isotype IgGs). An additional group of RM-1-Bhlhe22 was treated with GSK3326595. BMs were monitored using BLI and osteolytic lesions were quantified using micro-CT scan. Meanwhile, TRAP^{+}-osteoclasts were evaluated by TRAP staining (online supplemental figure 4J-L). At 30 days post-injection, the BM bone marrow was collected for flow cytometry analysis. Tumorous *Bhlhe22* overexpression strongly promoted CD11b^{+}Gr-1^{+} cells infiltration. However, *Prmt5* knockdown and Prmt5 inhibitor GSK3326595 treatment significantly inhibited CD11b^{+}Gr-1^{+} cells infiltration (figure 4L). In vitro, isolated mouse CD11b^{+}Gr-1^{+} cells were CFSE-labeled and co-cultured with RM-1-Vector or RM-1-Bhlhe22 or RM-1-Bhlhe22-Prmt5-sh cells (plus isotype IgGs). An additional co-culture group of RM-1-Bhlhe22 was treated with GSK591. At 5 days of incubation, CFSE assays showed that tumorous *Bhlhe22* overexpression strongly promoted CD11b^{+}Gr-1^{+} cells expansion. However, *Prmt5* knockdown and Prmt5 inhibitor GSK591 treatment significantly inhibited CD11b^{+}Gr-1^{+} cells expansion (figure 4M). Moreover, tumorous *Bhlhe22* overexpression significantly promotes and GSK591 significantly inhibited CD11b^{+}Gr-1^{+} cells proliferation (online supplemental figure 4M,N). Collectively, these results suggested that PRMT5 epigenetically activates *CSF2* expression and PRMT5 inhibition could reduce CD11b^{+}Gr-1^{+} cells infiltration.

CSF2 neutralization and ICT combination therapies effectively inhibit tumor-infiltrating immunosuppressive neutrophils and monocytes and BM in vivo

To explore the degree of resistance to PD-1 treatment caused by tumorous *Bhlhe22* overexpression, C57BL/6J BM mouse model was established using RM-1-Vector and RM-1-Bhlhe22 cells. Then, we treated RM-1-Vector group and RM-1-Bhlhe22 group with anti-PD-1 antibodies (isotype IgGs as control) (online supplemental figure 5A). Treatment with PD-1 alone could reduce the BM incidence and mortality of the Vector group. However, no significant improvement was observed in the Bhlhe22 group (online supplemental figure 5B-D). Interestingly, in vivo, we found tumorous *Bhlhe22* overexpression promoted osteoclasts formation. Anti-CSF2 and anti-Prmt5 significantly decreased the number of TRAP^{+} osteoclasts (online supplemental figure 3F,4L). To clarify BHLHE22 as a potential target for ICT therapy and exclude the effect of osteoclastogenesis, we performed an osteoclast inhibition experiment using zoledronic acid (online supplemental figure 5E). After osteoclasts inhibition, tumorous *Bhlhe22* overexpression could still significantly promote BM and osteolysis (online supplemental figure 5F,G). Thus, tumorous BHLHE22-induced dysregulation of the immune-microenvironment was the main driver in prostate cancer-derived bone metastases.

The expansion of intratumoral CD4^{+} T cells and the activation of cytotoxic CD8^{+} T cells determine the therapeutic efficacy of ICT.[29] The immunosuppressive microenvironment driven by CD11b^{+}Gr-1^{+} cell is one of the main reasons for the poor response of bone metastatic PCa to ICT, which prompted us to investigate whether

the inhibition of the BHLHE22/PRMT5/CSF2 pathway could improve the ICT response.

First, we tested our hypotheses in the C57BL/6J BM mouse model LCV-injected with RM-1-Bhlhe22 cells. Three days post-injection, we began treating mice with anti-CSF2 and/or anti-PD-1 antibodies (with isotype IgGs as a control) (figure 5A). BMs were monitored using BLI, and BM lesions were measured using micro-CT scan and TRAP staining (figure 5B,C).

The experiment was terminated at 70 days, and the incidence of BM was assessed. As to BM incidence, anti-CSF2 or anti-PD-1 antibodies alone showed no significant difference with the control. However, anti-CSF2 and anti-PD-1 combination therapy inhibited the occurrence of BM most effectively among all groups (figure 5D). Even so, in contrast to the rapidly progressing control group, treatment with anti-CSF2 or anti-PD-1 antibodies alone slowed down tumor progression and reduced the BM lesion area (figure 5E–G). Strikingly, among all treatment groups, the combination treatment group most effectively slowed down tumor progression and reduced the BM lesion area (figure 5E–G). Positive staining for the Ki-67 proliferation marker suggested that the combination treatment exerted potent tumor-growth retardation in mice (online supplemental figure 5H). Survival analysis demonstrated that the combination treatment group significantly prolonged the overall and BM-free survival (figure 5H1).

Subsequently, we further detected the infiltration of immunosuppressive neutrophils and monocytes, and T cells in the bone marrow using flow cytometry (figure 5J). Compared with the control group, anti-CSF2 alone decreased $CD11b^+Gr\text{-}1^+$ cell infiltration, and increased $CD4^+$ and $CD8^+$ T-cell infiltration, but could not promote the expansion of IFN-γ^+CD8^+ T cells (figure 5K–M). Anti-PD-1 alone promoted the expansion of IFN-γ^+CD8^+ T cells, but showed no significant effect on the infiltration of $CD11b^+Gr\text{-}1^+$ cells, $CD4^+$ and $CD8^+$ T cells (figure 5K–M). Notably, the combined treatment significantly decreased $CD11b^+Gr\text{-}1^+$ cell infiltration, increased $CD4^+$ and $CD8^+$ T-cell infiltration, and promoted the expansion of IFN-γ^+CD8^+ T cells (figure 5K–M). Collectively, these results indicated that combination of anti-CSF2 and anti-PD-1 antibodies effectively enhance the therapeutic efficacy of ICT for $BHLHE22^+$ PCa by relieving immunosuppression.

The PRMT5 inhibitor combined with ICT effectively inhibits tumor-infiltrating immunosuppressive neutrophils and monocytes and BM in vivo

Although CSF2 is a prospective therapeutic target for diverse cancers,[30 31] there is no validated CSF2 antagonists for clinical treatment. The PRMT5 inhibitor, GSK3326595, an oral PRMT5 inhibitor in a phase II clinical trial, enhances the response of cold (unresponsive) tumors to ICT.[32] Therefore, we further investigated the efficacy of GSK3326595 and ICT combination therapy.

PRMT5 inhibition significantly reduced the CSF2 expression and alleviated the immunosuppressive bone TME. Thus, we further explored whether the PRMT5 inhibitor combined with ICT could improve the efficacy of ICT. Three days post-injection, we began treating mice with GSK3326595 and/or anti-PD-1 antibodies (with isotype IgGs as a control) (figure 6A). BMs were monitored by BLI, and BM lesions were measured using micro-CT scan and TRAP staining (figure 6B,C).

The experiment was terminated at 70 days. In terms of BM incidence, GSK3326595 treatment alone showed no significant difference with the control. However, the combination treatment of GSK3326595 and anti-PD-1 effectively inhibited the occurrence of BM (figure 6D). GSK3326595 treatment alone slightly slowed down tumor progression and reduced the BM lesion area, similar to anti-PD-1 treatment alone (figure 6E–G). Impressively, the combination treatment most effectively slowed down tumor progression and reduced the BM lesion area (figure 6E–G). Ki-67 staining revealed that GSK3326595 plus anti-PD-1 combination treatment significantly inhibited the proliferation of tumor cells in BM lesions (online supplemental figure 5I). Survival analysis demonstrated that the combination treatment significantly prolonged the overall and BM-free survival (figure 6H1). Flow cytometry demonstrated that GSK3326595 treatment decreased $CD11b^+Gr\text{-}1^+$ cells infiltration and increased $CD4^+$ and $CD8^+$ T-cell infiltration (figure 6J–M). GSK3326595 combined with anti-PD-1 promoted the expansion of IFN-γ^+CD8^+ T cells (figure 6J–M). These results suggested that the combination of GSK3326595 and anti-PD-1 would effectively enhance the response of $BHLHE22^+$ PCa to ICT by relieving immunosuppression.

Potential role for BHLHE22 as a biomarker for ICT combination therapy in bone metastatic PCa

To assess the potential relevance of the BHLHE22/PRMT5/CSF2 axis and immune cell infiltration in human bone metastatic PCa, we examined the expression levels of BHLHE22, PRMT5, and CSF2 in our BM tissues using IHC (figure 7A). BHLHE22 staining was negative in 26.7% of BM samples, weak in 20% of BM samples, moderate in 23.3% of BM samples, and strong in 30% of BM samples (online supplemental figure 6A,B). Evidence indicates that PRMT5 is upregulated in PCa and acts as an oncogene for PCa cell growth.[33] Consistently, PRMT5 generally showed positive staining in BM tissues. Nevertheless, there was no significant difference in PRMT5 staining between the BHLHE22-low group and BHLHE22-high group (online supplemental figure 6C). Meanwhile, androgen receptor (AR) and neuroendocrine (NE) status were assessed to determine its distribution (online supplemental figure 6D,E and online supplemental table S1). Significantly, compared with that in the BHLHE22-low group, the BHLHE22-high group had higher $CD33^+$ cells counts, lower $CD4^+$ T and $CD8^+$ T cells infiltration per HPF(400×), and higher CSF2 expression (figure 7B,C). Positive staining for the Ki-67

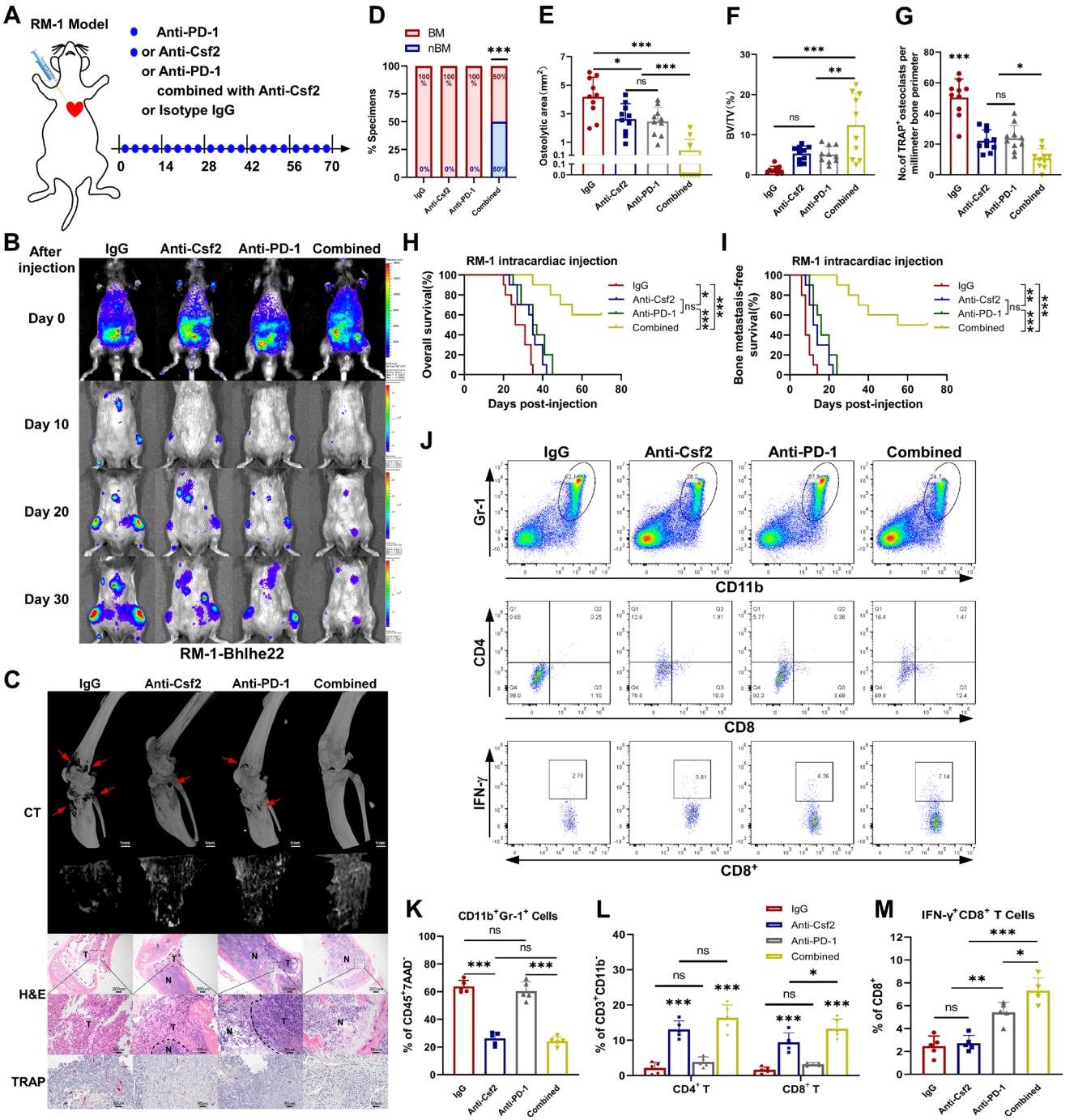

Figure 5 CSF2 neutralization and immune checkpoint therapy combination therapies effectively inhibit tumor-infiltrating immunosuppressive neutrophils and monocytes and bone metastasis in vivo. (A) The schedule of combination treatment in mice LCV-injected with RM-1-Bhlhe22 cells. The mice were treated with IgGs, anti-CSF2, anti-PD-1, or anti-PD-1 combined with anti-CSF2 (all n=10), beginning at day 3 post-injection. (B) Representative bioluminescent imaging signal of bone metastasis of LCV-injected C57BL/6J mice. (C) Representative micro-CT (arrows indicate osteolytic lesions. Bars, 1 mm), H&E (T, tumor; N, the adjacent non-tumor tissues. Bars, 200 µm and 50 µm) and TRAP (Bars, 50 µm) images of bone lesions. (D) Incidence of bone metastasis detected in the indicated groups. ***p<0.001; $\chi 2$ test. (E) Quantification of osteolytic areas in the indicated groups. ns, not significant. *p<0.05, ***p<0.001; one-way analysis of variance (ANOVA). (F) Quantification of bone parameters. BV/TV, bone/tissue volume ratio. ns, not significant. **p<0.01, ***p<0.001; one-way ANOVA. (G) Quantification of TRAP$^+$-osteoclastsin the indicated groups. ns, not significant. *p<0.05, ***p<0.001; one-way ANOVA. (H and I) Kaplan-Meier analysis of mouse overall (H) and bone metastasis-free (I) survival. ns, not significant. *p<0.05, **p<0.01, ***p<0.001; log-rank test. (J) Flow cytometry showing numbers of CD11b$^+$Gr-1$^+$ cells, CD4$^+$ T, CD8$^+$ T cells, and IFN-γ^+CD8$^+$ T cells. (K) to (M) Quantification of tumor-infiltrating CD11b$^+$Gr-1$^+$ cells (K), CD4$^+$ T, CD8$^+$ T cells (L), and IFN-γ^+CD8$^+$ T cells (M). ns, not significant. *p<0.05, **p<0.01, ***p<0.001; one-way ANOVA. BHLHE22, basic helix-loop-helix family member e22; BM, bone metastasis; nBM, without bone metastasis; CSF2, colony stimulating factor 2; IFN, interferon; LCV, left cardiac ventricle; PD-1, programmed cell death 1; TRAP, tartrate-resistant acid phosphatase.

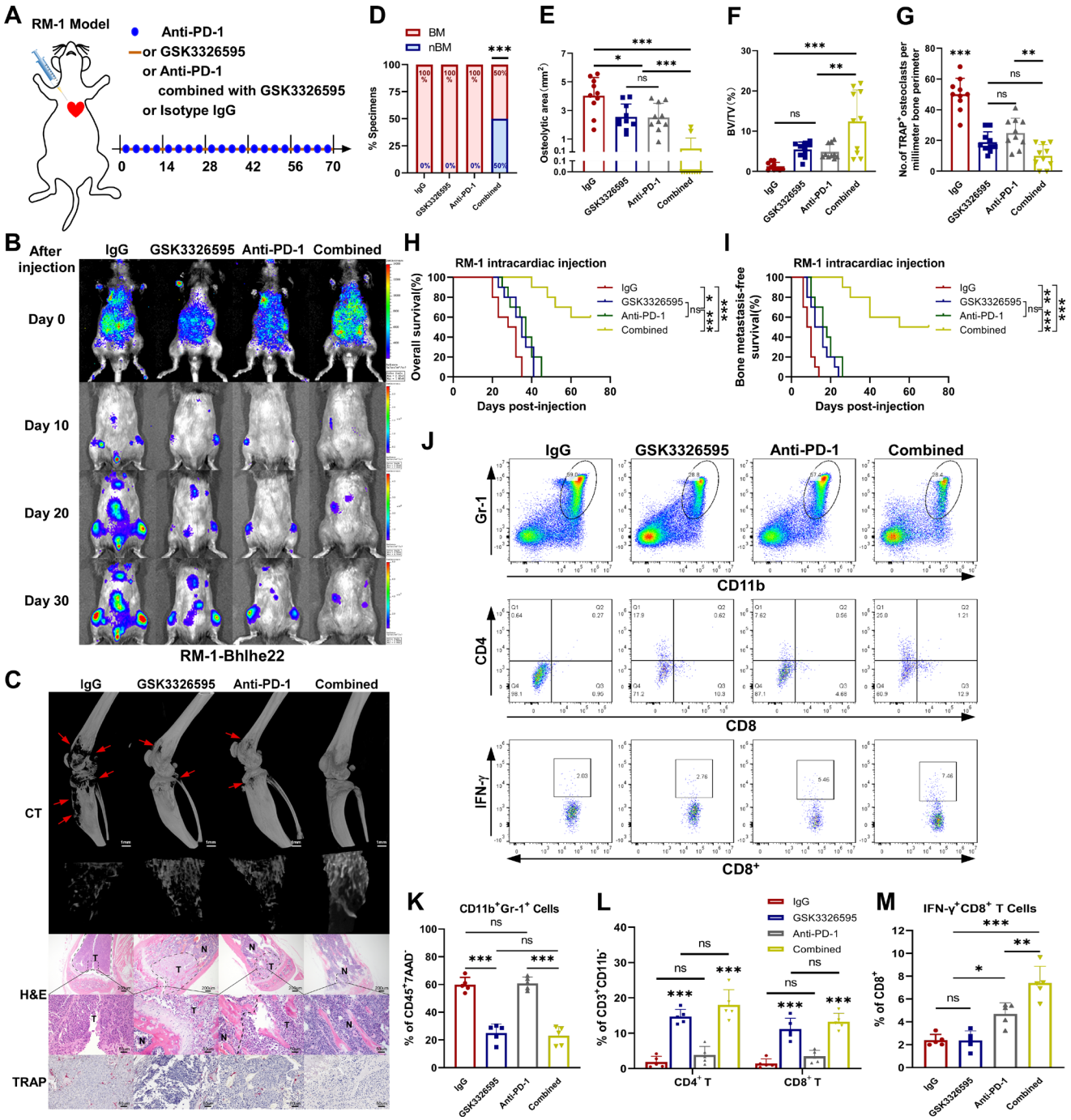

Figure 6 The protein arginine methyltransferase 5 inhibitor combined with immune checkpoint therapy effectively inhibits tumor-infiltrating immunosuppressive neutrophils and monocytes and bone metastasis in vivo. (A) The schedule of combination treatment in mice LCV- injected with RM-1-Bhlhe22 cells. The mice were treated with IgGs, GSK3326595, anti-PD-1, or anti-PD-1 combined with GSK3326595 (all n=10), beginning at day 3 post-injection. (B) Representative bioluminescent imaging signals of bone metastasis in LCV-injected C57BL/6J mice. (C) Representative micro-CT (arrows indicate osteolytic lesions. Bars, 1 mm), H&E (T, tumor; N, the adjacent non-tumor tissues. Bars, 200 µm and 50 µm) and TRAP (Bars, 50 µm) images of bone lesions. (D) Incidence of bone metastasis in the indicated groups. ***p<0.001; $\chi 2$ test. (E) Quantification of osteolytic areas in the indicated groups. ns, not significant. *p<0.05, ***p<0.001; one-way analysis of variance (ANOVA). (F) Quantification of bone parameters. BV/TV, bone/tissue volume ratio. ns, not significant. **p<0.01, ***p<0.001; one-way ANOVA. (G) Quantification of TRAP$^+$-osteoclasts in the indicated groups. ns, not significant. **p<0.01, ***p<0.001; one-way ANOVA. (H and I) Kaplan-Meier analysis of mouse overall (H) and bone metastasis-free (I) survivals. ns, not significant. *p<0.05, **p<0.01, ***p<0.001; log-rank test. (J) Flow cytometry showing numbers of CD11b$^+$Gr-1$^+$ cells, CD4$^+$ T, CD8$^+$ T cells, and IFN-γ^+CD8$^+$ T cells. (K) to (M) Quantification of tumor-infiltrating CD11b$^+$Gr-1$^+$ cells (K), CD4$^+$ T, CD8$^+$ T cells (L), and IFN-γ^+CD8$^+$ T cells (M). ns, not significant. *p<0.05, **p<0.01, ***p<0.001; one-way ANOVA. BHLHE22, basic helix-loop-helix family member e22; BM, bone metastasis; nBM, without bone metastasis; IFN, interferon; LCV, left cardiac ventricle; PD-1, programmed cell death 1; TRAP, tartrate-resistant acid phosphatase.

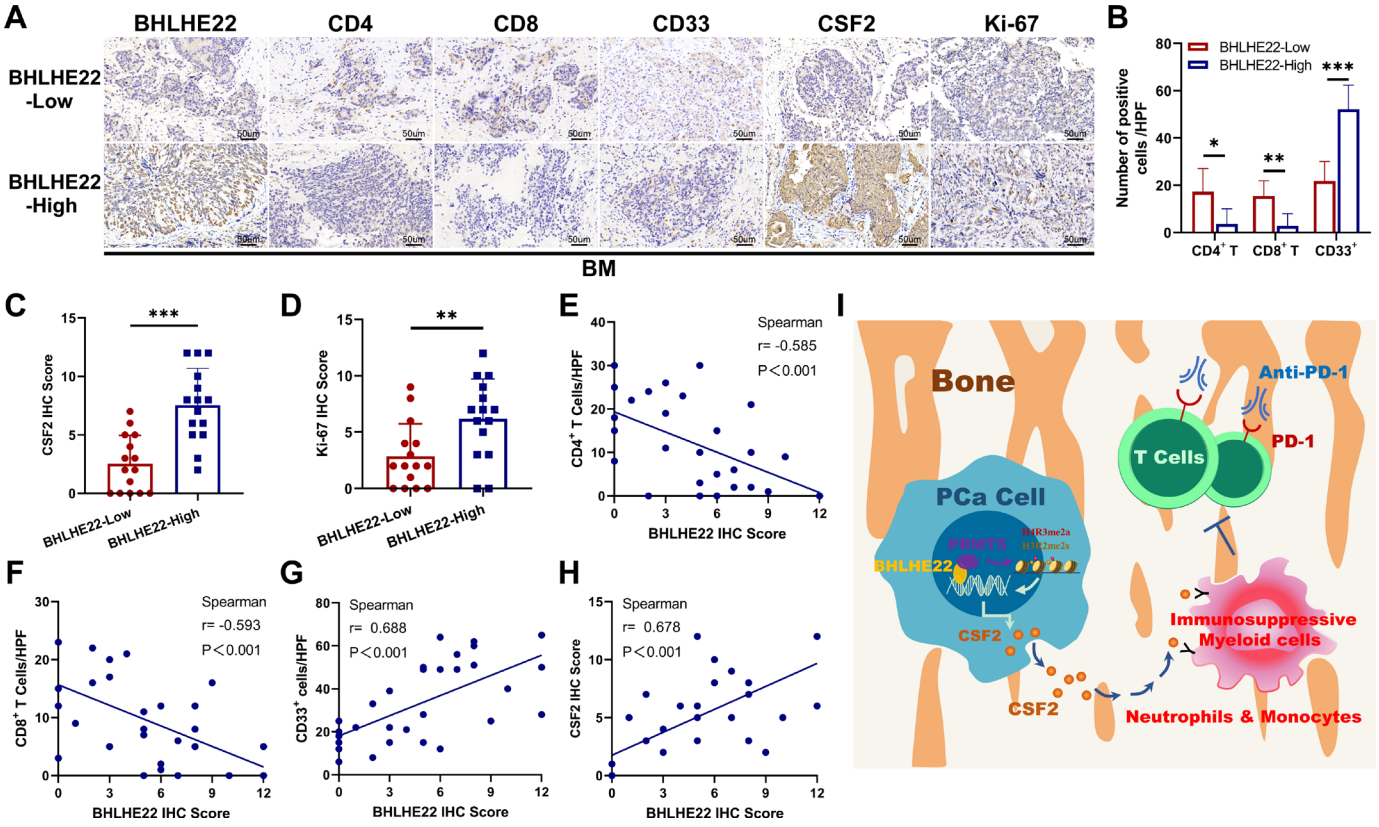

Figure 7 Potential role for BHLHE22 as a biomarker for immune checkpoint therapy combination therapies in bone metastatic PCa. (A) IHC results showing BHLHE22, CSF2, Ki-67 expression, and CD4$^+$ T (CD4), CD8$^+$ T (CD8), CD33$^+$ cells infiltration in BM samples from patients with PCa (n=30). Bars, 50 µm. (B) IHC results showing numbers of positive cells per high-power fields. *p<0.05, **p<0.01, ***p<0.001; t-test. (C and D) Histogram analysis of the staining score of CSF2 (C) and Ki-67 (D). **p<0.01, ***p<0.001; t-test. (E) to H) Spearman correlation analysis of numbers of CD4$^+$ T cells (E), CD8$^+$ T cells (F), CD33$^+$ cells (G) and CSF2 expression (H) with BHLHE22 expression, respectively. (I) Schematic diagram of BHLHE22$^+$ PCa cells driving an immunosuppressive bone tumor microenvironment and associated bone metastasis in PCa. BHLHE22, basic helix-loop-helix family member e22; BM, bone metastasis; CSF2, colony stimulating factor 2; IHC, immunohistochemical; PCa, prostate cancer.

proliferation marker suggested that BHLHE22 facilitated BM outgrowth in its unique bone TME (figure 7D). In addition, correlation analysis revealed that BHLHE22 correlated negatively with CD4$^+$ (r=−0.585, p<0.001; figure 7E) and CD8$^+$ T-cell infiltration (r=−0.593, p<0.001; figure 7F), but positively with CD33$^+$ cells infiltration (r=0.688, p<0.001; figure 7G) and CSF2 expression (r=0.678, p<0.001; figure 7H). Overall, our findings revealed the molecular mechanism responsible for the immunosuppressive bone TME and associated BM driven by the BHLHE22/PRMT5/CSF2 pathway in PCa (figure 7I). Targeting PRMT5/CSF2 combined with anti-PD-1 is a potential therapy for patients with BHLHE22$^+$ PCa.

DISCUSSION

The bone TME is a unique microenvironment conducive to the colonization, activation and growth of metastatic tumor cells.[3] Substantial evidence indicates that disturbance of normal bone homeostasis by tumor-derived factors forms an immunosuppressive microenvironment within the bone that favors disseminated tumor cells evading immune recognition and destruction.[29 34] In this process, immunosuppressive myeloid cells are recognized to play an important role in immune evasion of PCa cells.[35 36] Our study revealed that BHLHE22 drives an immunosuppressive bone TME by recruiting immunosuppressive neutrophils and monocytes, resulting in the increased expression and secretion of CSF2. Tumor-infiltrating immunosuppressive neutrophils and monocytes induce the formation of an immunosuppressive bone TME by exhausting CD4$^+$ T and CD8$^+$ T cells, which contributes to PCa cell BM. Mechanistically, BHLHE22 interacts with PRMT5 to form a transcriptional complex that epigenetically activates *CSF2* expression. More importantly, we demonstrated that BHLHE22 could serve as a novel biomarker to select the appropriate patients with bone metastatic PCa for ICT, and proposed a potential therapy to inhibit BM in patients with PCa.

BHLHE22 is a member of the bHLH transcription factor superfamily with highly specificity for DNA binding and tissue-specific expression.[18] The superfamily consists of BHLHE22, BHLHE23, and OLIG1-3.[18] BHLHE22 is widely expressed in pancreatic and neuronal cells, and is associated with neurodevelopment.[37 38] Interestingly, BHLHE22 was reported to be increased to a peak

in terminal neuroendocrine prostate cancer (NEPC) and is linked to cell fate specification.[19] Mechanistically, previous studies considered that BHLHE22 acts as a transcriptional repressor in the form of a dimerization complex. Meanwhile, BHLHE22 was believed to be unable to bind to DNA.[37] However, subsequent studies showed that Bhlhe22 could bind specifically to DNA and recruit Prdm8 to mediate transcriptional repression.[39] Our results demonstrated that BHLHE22 plays an important role in PCa BM. BHLHE22 is specifically upregulated in metastatic PCa bone tissues, and responsible for the enhancement of bone metastatic ability in PCa. Using co-IP assays and MS analysis, we found that Prmt5 interacts with Bhlhe22, but not with other bHLH family members. IF and IP assays proved the colocalization and interaction of Bhlhe22 and Prmt5 in RM-1-Bhlhe22 cells. Luciferase reporter assays and ChIP-qPCR indicated that Bhlhe22 transcriptionally activated *Csf2* expression. DNA pulldown and luciferase reporter assays with the mutated P1 verified that Bhlhe22 bound to the P1 region (sequence sites: 5′-CAAATATGCC-3′) of the *Csf2* promoter. Moreover, ChIP-qPCR suggested that Bhlhe22 and Prmt5 could bind to the *Csf2* promoter. *Prmt5* knockdown inhibited the binding of Prmt5 to the *Csf*2 promoter, but had no influence on Bhlhe22 binding. By contrast, lack of *Bhlhe22* expression strongly inhibited the binding of Prmt5 to the *Csf2* promoter. Thus, we considered that BHLHE22 had DNA binding ability and its transcriptional activity might depend on PRMT5 as the cofactor.

PRMT5 function as an epigenetic activator or repressor to regulate gene expression through methylating histones, and is broadly expressed in PCa.[27 40] The biological effects of PRMT5 methylation depend on its diverse catalytic substrates. H4R3, H3R2, and H3R8 are the most common catalytic substrates of PRMT5 in PCa.[28 33] Dimethylated histones H4R3me2s, H3R2me2a, and H3R8me2s are associated with transcriptional repression. In contrast, dimethylated histones H4R3me2a, H3R2me2s, and H3R8me2a are commonly associated with transcriptional activation.[27 28 33 40] Deng *et al* reported that PRMT5 was recruited to the *AR* promoter via its interaction with SP1 in PCa, resulting in epigenetic activation of *AR* expression.[33] Similarly, Beketova *et al* reported that PRMT5 cooperated with pICln and transcriptionally activated *AR* in PCa.[41] In this study, western blotting and qRT-PCR indicated that *Prmt5* knockdown decreased Csf2 expression. Meanwhile, the expression levels of H4R3me2a and H3R2me2s decreased significantly. Moreover, ChIP-qPCR suggested that the *Csf2* promoter could be precipitated using anti-H4R3me2a and anti-H3R2me2s antibodies in RM-1-Bhlhe22 cells, but not in RM-1-Bhlhe22-Prmt5-sh cells. In vivo and in vitro experiments showed that the transcriptional activation of *Csf2* was neutralized by *Prmt5* knockdown and Prmt5 antagonists (GSK3326595 and GSK591). Collectively, our study clarified that PRMT5 is part of the BHLHE22 transcriptional complex that epigenetically activates *CSF2* expression.

First-line ADT is the main treatment for patients with PCa.[42 43] However, the majority of advanced PCa will eventually progress to metastatic castration-resistant prostate cancer (mCRPC).[44 45] RM-1 cells are AR-negative mCRPC cell lines without NE traits (double-negative prostate cancer),[35] and their identification contributed to our understanding of the origin and therapeutic vulnerabilities of these cancers.[35] RNA-seq and qRT-PCR confirmed that wild-type RM-1 cell line lack *Bhlhe22* expression. Thus, we overexpressed *Bhlhe22* in RM-1 cell line. BHLHE22 was functionally linked to the progression and differentiation of PCa cells.[19] Similarly, enzalutamide-treated LNCaP cells had a higher level of BHLHE22 than untreated cells, and the highest expression was observed in NEPC cells (NCI-H660).[46] Hence, it remains to be further determined whether BHLHE22 is a downstream gene controlled by the AR signaling pathway.

Bone metastatic PCa is characterized by an immunosuppressive TME, resulting in a limited ICT response rate of 5%.[47] A recent clinical study designed specifically for patients with bone metastases reported that post-ICT evaluation of the bone microenvironment revealed transcriptional upregulation in myeloid and neutrophil immune subset signatures and increased expression of inhibitory immune checkpoints.[48] Strategies to alleviate immunosuppression mediated by immunosuppressive cell populations and secretory cytokines/chemokines might be effective in patients with bone metastatic PCa. Moreover, the essential steps include promoting the priming and activation of T cells, attracting and maintaining T-cell responses in tumor tissue, and establishing an immune-promoting TME.[34]

Myeloid-derived suppressor cells (MDSCs) have proven to be the cornerstone of the immunosuppressive TME, favoring immune escape and immunotherapy-resistance.[49] Theoretically, MDSCs are a heterogenous population of bone marrow-derived immature myeloid cells, including immunosuppressive neutrophils and monocytes. Although the pervasive use of the MDSC concept in tumor-immune research, the concept itself still implies the uncertainty of cellular identity.[21] Mechanistically, MDSCs express high levels of immunosuppressive factors, such as Arg-1 and inducible nitric oxide synthase, which lead to T-cell proliferation arrest.[20] Monocytic (M)-MDSCs produce higher amounts of Arg-1 and have stronger immunosuppressive competence than polymorphonuclear-MDSCs.[50 51] Previous studies have shown that the accumulation of MDSCs responds to chronic inflammation (including CSF1, CSF2, CSF3, and vascular endothelial growth factors (VEGFs)). Tumor-derived inflammatory factors trigger and maintain the prosperous state of MDSCs.[52 53] Ribechini *et al* demonstrated that myeloid cells expressing CSF2 were required for the conversion to M-MDSCs.[54] Consistent with these observations, CSF2 was identified as the critical mediator in our study.

The protumorigenic effects of immunosuppressive myeloid cells were dependent on dysfunction of adaptive

immune system and exhaustion of cytotoxic T lymphocytes. Further analyses confirmed that BHLHE22 expression level correlated positively with tumor-infiltrating immunosuppressive neutrophils and monocytes and negatively with tumor-infiltrating $CD4^+$ T and $CD8^+$ T cells. Meanwhile, $CD11b^+Gr\text{-}1^+$ cells expansion resulted in decreased levels of tumor-infiltrating IFN-γ^+CD8^+ T cells and increased levels of tumor-infiltrating PD-1^+CD8^+ T cells. $CD11b^+Gr\text{-}1^+$ cells depletion assays suggested that the exhaustion of T cells could be reversed. Moreover, flow cytometry demonstrated that the $CD11b^+Gr\text{-}1^+$ cells with high amounts of Arg-1 were the main 'protectors' of $BHLHE22^+$ PCa cells, especially immunosuppressive monocytes.

To improve the response rate of ICT, various combined regimens have been examined in preclinical studies. The inhibition of pY696-EZH2 with an Src inhibitor enhanced the therapeutic efficacy of ICT in deterring brain metastases by decreasing the numbers of immunosuppressive neutrophils.[55] A CXCR2 inhibitor significantly enhanced the immune response and prolonged survival in ICT-resistant colorectal cancer driven by MDSCs.[56] ETS homologous factor (EHF) induced the accumulation of MDSCs via pancreatic tumor-derived transforming growth factor-β and CSF2, reducing the beneficial effect of ICT.[30] In terms of PCa treatment, the inhibition of CSF1, IL-6, PI3Kα/β, and CXCR2 relieved MDSC-mediated immunosuppression and significantly enhanced the antitumor effects of ICT.[57–60] Eradicating $CD11b^+Gr\text{-}1^+$ cells could improve the efficacy of cancer immunotherapy. In our study, we examined the efficacy of combination treatment of anti-CSF2 plus anti-PD-1 and GSK3326595 plus anti-PD-1, respectively. Overall and BM-free survival were both significantly increased by the two combination regimens. Flow cytometry analysis demonstrated that the infiltration of $CD11b^+Gr\text{-}1^+$ cells decreased significantly; however, the infiltration of $CD4^+$ T and $CD8^+$ T cells increased significantly. Meanwhile, a transition from an immunosuppressed to immunoactivated phenotype was exhibited in $CD8^+$ T cells. Moreover, BHLHE22 correlated positively with the number of $CD33^+$ cells and CSF2 expression, and correlated negatively with the number of $CD4^+$ T and $CD8^+$ T cells in PCa tissue samples. Thus, these results highlighted a novel strategy for patient selection and treatment to reduce ICT resistance in bone metastatic PCa.

In summary, we clarified the immunosuppressive mechanism of tumorous BHLHE22 in bone metastatic PCa. BHLHE22 coupled with PRMT5 forms a transcriptional complex that epigenetically activates *CSF2* expression, which is the critical suppressive cytokine involved in the accumulation of immunosuppressive neutrophils and monocytes. Tumorous BHLHE22 is a promising biomarker for patient selection to enhance the efficacy of anti-PD-1 therapy. The combination of anti-CSF2/anti-PRMT5 and anti-PD-1 represent prospective therapies for patients with PCa with $BHLHE22^+$ and bone metastases.

Author affiliations
[1]Department of Orthopaedic Surgery, Sun Yat-sen University First Affiliated Hospital, Guangzhou, Guangdong, China
[2]Orthopaedic Research Institute, Guangdong Provincial Key Laboratory of Orthopedics and Traumatology, Guangzhou, Guangdong, China
[3]Department of Gastrointestinal Surgery, Sun Yat-sen University First Affiliated Hospital, Guangzhou, Guangdong, China
[4]Department of Pathology, the First People's Hospital of Guangzhou City, Guangzhou, Guangdong, China

Contributors XP, YD, CL, and CY developed the original idea and designed the experiments. CY prepared the figures and drafted the manuscript. CY, MW, YW, QL, and KL conducted the experiments and contributed to data analysis. XP and HD provided critical reagents and/or clinical samples. XP and YD supervised the study. All authors contributed to revising the manuscript and approved the final version for publication. XP is responsible for the overall content as the guarantor.

Funding This work was supported by grants from the National Natural Science Foundation of China (grant numbers 81872176, 82072973, 81902735) and the Basic and Applied Basic Research Foundation of Guang-dong province (grant numbers 2019A1515010342).

Competing interests None declared.

Patient consent for publication Not applicable.

Ethics approval The use of specimens and the patients' clinical information was approved by the Institutional Research Ethics Committee of The First Affiliated Hospital of Sun Yat-sen University ((2014)A-011). Participants gave informed consent to participate in the study before taking part.

Provenance and peer review Not commissioned; externally peer reviewed.

Data availability statement Data are available in a public, open access repository. Data are available on reasonable request. The sequencing data and processed expression matrix have been deposited at the Gene Expression Omnibus with access number GSE201381 and GSE206108.

ORCID iD
Xinsheng Peng http://orcid.org/0000-0002-4377-3703

REFERENCES

1 Coleman RE, Croucher PI, Padhani AR, *et al*. Bone metastases. *Nat Rev Dis Primers* 2020;6:83.
2 Sowder ME, Johnson RW. Bone as a preferential site for metastasis. *JBMR Plus* 2019;3:e10126.
3 Ren D, Dai Y, Yang Q, *et al*. Wnt5A induces and maintains prostate cancer cells dormancy in bone. *J Exp Med* 2019;216:428–49.
4 Croucher PI, McDonald MM, Martin TJ. Bone metastasis: the importance of the neighbourhood. *Nat Rev Cancer* 2016;16:373–86.
5 Siegel RL, Miller KD, Fuchs HE, *et al*. Cancer statistics, 2022. *CA Cancer J Clin* 2022;72:7–33.
6 Kfoury Y, Baryawno N, Severe N, *et al*. Human prostate cancer bone metastases have an actionable immunosuppressive microenvironment. *Cancer Cell* 2021;39:1464–78.
7 Halabi S, Kelly WK, Ma H, *et al*. Meta-Analysis evaluating the impact of site of metastasis on overall survival in men with castration-resistant prostate cancer. *J Clin Oncol* 2016;34:1652–9.

8 Teo MY, Rathkopf DE, Kantoff P. Treatment of advanced prostate cancer. *Annu Rev Med* 2019;70:479–99.
9 Weilbaecher KN, Guise TA, McCauley LK. Cancer to bone: a fatal attraction. *Nat Rev Cancer* 2011;11:411–25.
10 Mateo J, McKay R, Abida W, *et al*. Accelerating precision medicine in metastatic prostate cancer. *Nat Cancer* 2020;1:1041–53.
11 Gartrell BA, Coleman R, Efstathiou E, *et al*. Metastatic prostate cancer and the bone: significance and therapeutic options. *Eur Urol* 2015;68:850–8.
12 McDermott DF, Sosman JA, Sznol M, *et al*. Atezolizumab, an anti-programmed death-ligand 1 antibody, in metastatic renal cell carcinoma: long-term safety, clinical activity, and immune correlates from a phase Ia study. *J Clin Oncol* 2016;34:833–42.
13 Le DT, Durham JN, Smith KN, *et al*. Mismatch repair deficiency predicts response of solid tumors to PD-1 blockade. *Science* 2017;357:409–13.
14 Palena C, Gulley JL. A rare insight into the immunosuppressive landscape of prostate cancer bone metastases. *Cancer Cell* 2021;39:1450–2.
15 Chen DS, Mellman I. Elements of cancer immunity and the cancer-immune set point. *Nature* 2017;541:321–30.
16 Beer TM, Kwon ED, Drake CG, *et al*. Randomized, double-blind, phase III trial of ipilimumab versus placebo in asymptomatic or minimally symptomatic patients with metastatic chemotherapy-naive castration-resistant prostate cancer. *J Clin Oncol* 2017;35:40–7.
17 Powles T, Yuen KC, Gillessen S, *et al*. Atezolizumab with enzalutamide versus enzalutamide alone in metastatic castration-resistant prostate cancer: a randomized phase 3 trial. *Nat Med* 2022;28:144–53.
18 Peyton M, Stellrecht CM, Naya FJ, *et al*. Beta3, a novel helix-loop-helix protein, can act as a negative regulator of beta2 and MyoD-responsive genes. *Mol Cell Biol* 1996;16:626–33.
19 Akamatsu S, Wyatt AW, Lin D, *et al*. The placental gene PEG10 promotes progression of neuroendocrine prostate cancer. *Cell Rep* 2015;12:922–36.
20 Bronte V, Brandau S, Chen S-H, *et al*. Recommendations for myeloid-derived suppressor cell nomenclature and characterization standards. *Nat Commun* 2016;7:12150.
21 Alshetaiwi H, Pervolarakis N, McIntyre LL, *et al*. Defining the emergence of myeloid-derived suppressor cells in breast cancer using single-cell transcriptomics. *Sci Immunol* 2020;5:eaay6017.
22 Nagarsheth N, Wicha MS, Zou W. Chemokines in the cancer microenvironment and their relevance in cancer immunotherapy. *Nat Rev Immunol* 2017;17:559–72.
23 MacDonald BR, Mundy GR, Clark S, *et al*. Effects of human recombinant CSF-GM and highly purified CSF-1 on the formation of multinucleated cells with osteoclast characteristics in long-term bone marrow cultures. *J Bone Miner Res* 1986;1:227–33.
24 Khan A, Fornes O, Stigliani A, *et al*. JASPAR 2018: update of the open-access database of transcription factor binding profiles and its web framework. *Nucleic Acids Res* 2018;46:D1284.
25 Weirauch MT, Yang A, Albu M, *et al*. Determination and inference of eukaryotic transcription factor sequence specificity. *Cell* 2014;158:1431–43.
26 Xu Z-P, Dutra A, Stellrecht CM, *et al*. Functional and structural characterization of the human gene BHLHB5, encoding a basic helix-loop-helix transcription factor. *Genomics* 2002;80:311–8.
27 Beketova E, Owens JL, Asberry AM, *et al*. Prmt5: a putative oncogene and therapeutic target in prostate cancer. *Cancer Gene Ther* 2022;29:264–76.
28 Kim H, Ronai ZA. Prmt5 function and targeting in cancer. *Cell Stress* 2020;4:199–215.
29 Jiao S, Subudhi SK, Aparicio A, *et al*. Differences in tumor microenvironment dictate T helper lineage polarization and response to immune checkpoint therapy. *Cell* 2019;179:1177–90.
30 Liu J, Jiang W, Zhao K, *et al*. Tumoral EHF predicts the efficacy of anti-PD1 therapy in pancreatic ductal adenocarcinoma. *J Exp Med* 2019;216:656–73.
31 Zhang C-X, Ye S-B, Ni J-J, *et al*. Sting signaling remodels the tumor microenvironment by antagonizing myeloid-derived suppressor cell expansion. *Cell Death Differ* 2019;26:2314–28.
32 Kim H, Kim H, Feng Y, *et al*. Prmt5 control of cgas/STING and NLRC5 pathways defines melanoma response to antitumor immunity. *Sci Transl Med* 2020;12:eaaz5683.
33 Deng X, Shao G, Zhang H-T, *et al*. Protein arginine methyltransferase 5 functions as an epigenetic activator of the androgen receptor to promote prostate cancer cell growth. *Oncogene* 2017;36:1223–31.
34 O'Donnell JS, Teng MWL, Smyth MJ. Cancer immunoediting and resistance to T cell-based immunotherapy. *Nat Rev Clin Oncol* 2019;16:151–67.
35 Su W, Han HH, Wang Y, *et al*. The polycomb repressor complex 1 drives double-negative prostate cancer metastasis by coordinating stemness and immune suppression. *Cancer Cell* 2019;36:139–55.
36 Lu X, Horner JW, Paul E, *et al*. Effective combinatorial immunotherapy for castration-resistant prostate cancer. *Nature* 2017;543:728–32.
37 Kim MH, Gunnersen J, Augustine C, *et al*. Region-Specific expression of the helix-loop-helix gene beta3 in developing and adult brains. *Mech Dev* 2002;114:125–8.
38 Skaggs K, Martin DM, Novitch BG. Regulation of spinal interneuron development by the olig-related protein bhlhb5 and Notch signaling. *Development* 2011;138:3199–211.
39 Ross SE, McCord AE, Jung C, *et al*. Bhlhb5 and Prdm8 form a repressor complex involved in neuronal circuit assembly. *Neuron* 2012;73:292–303.
40 Yuan Y, Nie H. Protein arginine methyltransferase 5: a potential cancer therapeutic target. *Cell Oncol (Dordr)* 2021;44:33–44.
41 Beketova E, Fang S, Owens JL, *et al*. Protein arginine methyltransferase 5 promotes picln-dependent androgen receptor transcription in castration-resistant prostate cancer. *Cancer Res* 2020;80:4904–17.
42 Agarwal N, Sonpavde G, Sternberg CN. Novel molecular targets for the therapy of castration-resistant prostate cancer. *Eur Urol* 2012;61:950–60.
43 Davis ID, Martin AJ, Stockler MR, *et al*. Enzalutamide with standard first-line therapy in metastatic prostate cancer. *N Engl J Med* 2019;381:121–31.
44 Chen WS, Aggarwal R, Zhang L, *et al*. Genomic drivers of poor prognosis and enzalutamide resistance in metastatic castration-resistant prostate cancer. *Eur Urol* 2019;76:562–71.
45 Isaacsson Velho P, Fu W, Wang H, *et al*. Wnt-pathway activating mutations are associated with resistance to first-line abiraterone and enzalutamide in castration-resistant prostate cancer. *Eur Urol* 2020;77:14–21.
46 Ci X, Hao J, Dong X, *et al*. Heterochromatin protein 1α mediates development and aggressiveness of neuroendocrine prostate cancer. *Cancer Res* 2018;78:2691–704.
47 Antonarakis ES, Piulats JM, Gross-Goupil M, *et al*. Pembrolizumab for treatment-refractory metastatic castration-resistant prostate cancer: multicohort, open-label phase II KEYNOTE-199 study. *J Clin Oncol* 2020;38:395–405.
48 Subudhi SK, Siddiqui BA, Aparicio AM, *et al*. Combined CTLA-4 and PD-L1 blockade in patients with chemotherapy-naïve metastatic castration-resistant prostate cancer is associated with increased myeloid and neutrophil immune subsets in the bone microenvironment. *J Immunother Cancer* 2021;9:e002919.
49 Tesi RJ. Mdsc; the most important cell you have never heard of. *Trends Pharmacol Sci* 2019;40:4–7.
50 Dolcetti L, Peranzoni E, Ugel S, *et al*. Hierarchy of immunosuppressive strength among myeloid-derived suppressor cell subsets is determined by GM-CSF. *Eur J Immunol* 2010;40:22–35.
51 Kumar V, Patel S, Tcyganov E, *et al*. The nature of myeloid-derived suppressor cells in the tumor microenvironment. *Trends Immunol* 2016;37:208–20.
52 Veglia F, Perego M, Gabrilovich D. Myeloid-Derived suppressor cells coming of age. *Nat Immunol* 2018;19:108–19.
53 Ushach I, Zlotnik A. Biological role of granulocyte macrophage colony-stimulating factor (GM-CSF) and macrophage colony-stimulating factor (M-CSF) on cells of the myeloid lineage. *J Leukoc Biol* 2016;100:481–9.
54 Ribechini E, Hutchinson JA, Hergovits S, *et al*. Novel GM-CSF signals via IFN-γr/IRF-1 and Akt/mTOR license monocytes for suppressor function. *Blood Adv* 2017;1:947–60.
55 Zhang L, Yao J, Wei Y, *et al*. Blocking immunosuppressive neutrophils deters py696-EZH2-driven brain metastases. *Sci Transl Med* 2020;12:eaaz5387.
56 Liao W, Overman MJ, Boutin AT, *et al*. KRAS-IRF2 axis drives immune suppression and immune therapy resistance in colorectal cancer. *Cancer Cell* 2019;35:559–72.
57 Zhao D, Cai L, Lu X, *et al*. Chromatin regulator Chd1 remodels the immunosuppressive tumor microenvironment in PTEN-deficient prostate cancer. *Cancer Discov* 2020;10:1374–87.
58 Qi Z, Xu Z, Zhang L, *et al*. Overcoming resistance to immune checkpoint therapy in PTEN-null prostate cancer by intermittent anti-pi3kα/β/δ treatment. *Nat Commun* 2022;13:182.
59 Garcia AJ, Ruscetti M, Arenzana TL, *et al*. Pten null prostate epithelium promotes localized myeloid-derived suppressor cell expansion and immune suppression during tumor initiation and progression. *Mol Cell Biol* 2014;34:2017–28.
60 Wang G, Lu X, Dey P, *et al*. Targeting YAP-dependent MDSC infiltration impairs tumor progression. *Cancer Discov* 2016;6:80–95.